# TOMBALL TECHNOLOGY CENTER

*Geomechanics*

## EQUITABLE PRODUCTION CO.
## STATIC AND DYNAMIC ELASTIC PROPERTIES OF WEIR SANDSTONE CORES FROM THE KANAWHA #1641 WELL

**TECHNOLOGY CENTER REPORT NO. 04-02-0104**

**BJ SERVICES TECHNICAL REPRESENTATIVE**

**MR. ROGER MYERS**

**PITTSBURGH, PA**

**OCTOBER 4, 2004**

## EXECUTIVE SUMMARY

Young's Modulus and Poisson's Ratio were measured on Weir sandstone cores from two distinct depth intervals (1967 feet and 2021 feet). Both static and dynamic testing methods were used in determining the elastic properties of these cores. All tests were conducted on dry core placed under a triaxial state of stress and at room temperature.

Results indicated that the average static Young's modulus averaged $2.85 \times 10^6$ psi among cores from the 1966'-1967 feet upper sand that contained no calcite, $3.97 \times 10^6$ psi among the core from 1967 feet that contained calcite, and $2.67 \times 10^6$ psi among cores that came from 2021 feet. The average static Poisson's Ratio ranged from 0.06 in the lower sand interval to 0.14 in the upper sand interval. Fair to good correlations were found between the static Young's modulus and bulk density, p-wave transit time, and the dynamic Young's modulus. A good correlation was also found between the shear wave and p-wave transit times. No relation between static and dynamic Poisson's Ratio was observed, although the static values were lower than the dynamic values by a factor ranging from 0.27 to 0.65.

## INTRODUCTION

This report contains the test results of mechanical property measurements on Weir sandstone formation cores. This work was requested to assist in the evaluation of potential hydraulic fracture treatment designs. In addition to the mechanical property measurements, mineralogical (XRD) and scanning electron microscopy analyses were performed and separately reported[1].

Specifically, Young's modulus and Poisson's Ratio were measured using conventional static and dynamic testing methods. All tests were conducted at room temperature on dry samples under a triaxial state of stress. These elastic parameters are required input data for current hydraulic fracture models. The magnitudes of the moduli influence fracture width and to some extent fracture height, while contrasts in elastic properties between zones have been used to identify zones that inhibited fracture height growth.

The most reliable way to obtain the elastic moduli is to directly measure these properties on cored materials under in-situ test conditions. However, cores are not acquired in every well, and where they are acquired, the sampling is often sparse. On the other hand, sonic-density logs acquire the elastic properties continuously with depth under in-situ conditions. Unfortunately, these values tend to be greater than those measured on cores using conventional static test apparatus. Therefore, dynamic elastic moduli obtained from logs often have to be converted to their "static" values through either published or local correlation functions. In order to facilitate a static/dynamic transform, both the dynamic and static Young's moduli and Poisson's Ratios were measured and comparisons between dynamic and static elastic properties are presented. The comparisons between static and dynamic elastic properties are meant to serve only as a guide for deriving an empirical transform for log-based measurements. Static/dynamic transforms presented in this report should be verified with wireline-log calibrated data before applying to field situations.

## SAMPLE DESCRIPTIONS

Thirteen (13) sandstone cores were sent to TTC for testing. All samples were received in good condition. The cores came from two distinct depth intervals: upper sand interval from 1966 feet to 1967.5 feet; lower sand interval from 2021 feet to 2022 feet. Within the upper sand interval, there was a hard streak of core at 1067.4 feet (Samples I and J) with higher than normal bulk densities.

XRD analysis of these sands showed quartz to be the major constituent in the upper and lower sands. Sample J contained a high percentage (31%) of calcite. This mineral is most likely the cause of the higher than normal bulk densities observed in Samples I and J. Clay content in all cores was low ranging from 4% to 9%. There were also low concentrations of feldspars (2% - 7%). An inventory of the cores is presented in Table 1.

Table 1
Inventory of Weir Sandstone Cores

| Sample | Depth (ft) | Length (in.) | Diameter (in.) | Bulk Density (g/cc) | Porosity* (%) | Air Perm* (mD) |
|---|---|---|---|---|---|---|
| A | 1966 | 1.325 | 0.968 | 2.435 | 10.4 | 0.366 |
| B | 1966.1 | 1.791 | 0.967 | 2.374 | 12.4 | 1.742 |
| C | 1966.2 | 1.682 | 0.964 | 2.396 | 12.2 | 1.129 |
| D | 1966.8 | 1.582 | 0.964 | 2.582 | 8.6 | 2.709 |
| E | 1966.9 | 1.826 | 0.963 | 2.429 | 10.2 | 0.229 |
| F | 1967 | 1.846 | 0.965 | 2.443 | 9.4 | 0.119 |
| G | 1967.1 | 1.842 | 0.965 | 2.450 | 9.4 | 0.764 |
| H | 1967.3 | 1.788 | 0.966 | 2.478 | 8.2 | 0.079 |
| I | 1967.4 | 1.377 | 0.965 | 2.684 | 2.3 | 0.000 |
| J | 1967.5 | 1.422 | 0.967 | 2.724 | 1.6 | 0.000 |
| K | 2021 | 1.584 | 0.964 | 2.495 | 7.2 | 0.122 |
| L | 2021.2 | 1.572 | 0.961 | 2.491 | 8.1 | 0.730 |
| M | 2022 | 1.741 | 0.959 | 2.325 | 14.0 | 1.979 |

* see TTC Report #04-02-0104[1]

## RESULTS AND INTERPRETATION

### Dynamic Elastic Properties

The dynamic elastic properties were measured using a standard through-transmission pulsed ultrasonic technique. Details of the test procedures are discussed in the next section. In short, the dynamic elastic moduli (Young's modulus and Poisson's Ratio) were calculated from measurements of the compressional and shear wave velocities and bulk density using Equations (9) and (10). The wave velocities were measured at reservoir net mean stress. The results are displayed in Table 2. The stress-dependent wave velocity data are located in Appendix I.

The reservoir net mean stress was estimated from assumed values of overburden stress, closure stress, and reservoir pressure gradients of 1.0 psi/ft and 0.7 psi/ft, and 0.45 psi/ft, respectively. The reservoir net mean stress was calculated from the expression:

$$\sigma'_m = [(G_o + 2G_c)/3 - \alpha G_p]D \qquad (1)$$

The letter "G" represents the gradient. $\alpha$ is the poro-elastic constant, and was assumed equal to 0.8. D is depth (in feet), and the subscripts, o, c, p, and m, represent the overburden, closure, reservoir pressure, and mean stress, respectively. Core depths ranged from 1966 feet to 202 feet. As a result, the reservoir net mean stress ranged from 865 psi to 890 psi. Consequently, the confining stress used in these tests was set to 900 psi.

The results in Table 2 were divided into three groups:

(1) Samples A-H, which came from the upper sand interval and had bulk densities ranging from 2.43 g/cc to 2.58 g/cc;
(2) Samples I-J which had bulk densities ranging from 2.68 g/cc to 2.72 g/cc;
(3) Samples K-M, which came from the lower sand interval and had bulk densities ranging from 2.32 g/cc to 2.49 g/cc.

Table 2 also presents the average values and standard deviations of the elastic properties for each group. The compressional and shear wave transit times of the lower bulk density upper and lower sands were nearly identical, which resulted in nearly identical dynamic moduli. The higher density, calcite-rich cores had significantly shorter transit times and greater Young's moduli than the other cores. There was very little variation in Poisson's Ratio, on average, between the three sets of core.

Static Elastic Properties

The static elastic moduli were measured using procedures discussed in the next section. These moduli were measured concurrent with the dynamic elastic moduli. The results are presented in Table 3. The average Young's modulus of Samples A-H, I-J, and K-M were $2.85 \times 10^6$ psi, $3.97 \times 10^6$ psi, and $2.67 \times 10^6$ psi, respectively. The average Poisson's Ratio of the above grouping of samples were 0.12, 0.14, and 0.06, respectively.

Again, the data was divided into groups as discussed above. As might have been expected, the static Young's moduli of the higher density cores (Samples I-J) were significantly greater than the moduli of the lower density cores. Poisson's Ratio varied more between the upper and lower sands than between high and low density cores. If it is true that calcite is responsible for enhancing the magnitude of Young's modulus, then calcite-rich intervals throughout this formation should produce narrower fracture widths and possibly exist at greater minimum principle stresses. If thick enough, the calcite-rich intervals may also provide some resistance to fracture height growth.

Empirical Relations between Static and Dynamic Elastic Properties

This section presents analyses using data presented in Tables 2 and 3 that attempted to find empirical relations between various quantities that may assist in estimating the static moduli from more commonly acquired data and in calibrating current wireline-derived mechanical property logs. The relations discussed in this section are meant to serve only as a guide for identifying those quantities that might correlate strongly with the static and dynamic elastic moduli.

Figure 1 presents a cross-plot of the static Young's modulus versus bulk density of the core samples. A linear regression was performed on all the data points that resulted in the following expression.

$$E_s = 3.495\rho_b - 5.70 \quad (2)$$

$\rho_b$ is the bulk density expressed in units of g/cc and $E_s$ is Young's modulus expressed in millions of pounds per square inch (Mpsi). The correlation was fair (i.e. $R^2 = 0.71$), which was due mostly to the calcite-rich cores. Such a relation may be useful in wells where a density log had been run, but not a sonic log.

Figure 2 displays a cross-plot of static Young's modulus versus the p-wave transit time. Again, the data appeared to follow a linear trend, and a linear regression to all the data was performed resulting in the following expression.

$$E_s = 9.44 - 0.091(1/V_p) \quad (3)$$

$1/V_p$ is the p-wave transit time expressed in units of μsec/ft. The correlation was relatively good, and suggests that the p-wave transit times from sonic logs should provide a good estimate to the static modulus.

Figure 3 displays a cross-plot of static versus dynamic Young's modulus. A linear regression was again performed on the data resulting in the following expression.

$$E_s = 0.40E_{dyn} + 0.539 \quad (4)$$

This correlation was good, as one might have expected, because of the relatively good correlations that had been found between the static Young's modulus and bulk density and p-wave transit time.

Figure 4 displays a cross-plot between the static and dynamic Poisson's Ratio. As is typically found, there was no obvious correlation between the two quantities. It is clear from the plot that dynamic values were greater than the static values. A calculation of the average ratio of the static to dynamic Poisson's Ratio was performed. The results are shown below.

$$\langle \nu_s/\nu_{dyn} \rangle = 0.65\ (\pm\ 0.22) \text{ for samples A-H} \quad (5)$$

$$\langle v_s/v_{dyn} \rangle = 0.57 \text{ for sample J} \quad (6)$$

$$\langle v_s/v_{dyn} \rangle = 0.27 (\pm 0.15) \text{ for samples K-M} \quad (7)$$

The quantities in parenthesis are the standard deviations of the set of measurements.

Figure 5 displays a cross-plot of shear wave versus p-wave transit times. The data appeared to follow a linear trend. A linear regression of the data was performed resulting in the following expression:

$$1/V_s = 18.8 + 1.37(1/V_p) \quad (8)$$

There was a good correlation between these two quantities as observed by the $R^2$-coefficient. These results suggest that the s-wave transit time can be estimated in wells where there exists p-wave transit time data (DTC log), but not a shear wave data. Consequently, the dynamic Poisson's Ratio could then be estimated using only p-wave transit times.

In summary, the average static Young's modulus averaged $2.85 \times 10^6$ psi among cores from the 1966'-1967 feet upper sand that contained no calcite, $3.97 \times 10^6$ psi among the core from 1967 feet that contained calcite, and $2.67 \times 10^6$ psi among cores that came from 2021 feet. The average static Poisson's Ratio ranged from 0.06 in the lower sand interval to 0.14 in the upper sand interval. Fair to good correlations were found between the static Young's modulus and bulk density, p-wave transit time, and the dynamic Young's modulus. A good correlation was also found between the shear and p-wave transit times.

Table 2
Dynamic Elastic Properties of Weir Sandstone

| Sample | Depth (ft) | Poisson's Ratio | Young's Modulus ($x10^6$ psi) | Inverse P-Wave Velocity (μsec/ft) | Inverse S-Wave Velocity (μsec/ft) |
|---|---|---|---|---|---|
| A | 1966 | 0.197 | 5.17 | 75.7 | 123.3 |
| B | 1966.1 | 0.198 | 5.33 | 73.6 | 119.8 |
| C | 1966.2 | 0.144 | 5.71 | 73.3 | 113.7 |
| D | 1966.8 | 0.198 | 5.70 | 74.2 | 120.9 |
| E | 1966.9 | 0.194 | 5.95 | 70.6 | 114.6 |
| F | 1967 | 0.194 | 6.22 | 69.3 | 112.4 |
| G | 1967.1 | 0.184 | 5.37 | 75.0 | 120.6 |
| H | 1967.3 | 0.229 | 6.26 | 67.9 | 114.5 |
| Average → | | **0.19** | **5.72** | **72.4** | **117.5** |
| Stdev. → | | **0.02** | **0.41** | **2.8** | **4.1** |
| I | 1967.4 | 0.184 | 8.47 | 62.6 | 100.5 |
| J | 1967.5 | 0.248 | 8.65 | 59.6 | 102.9 |
| Average → | | **0.22** | **8.56** | **61.1** | **101.7** |
| Stdev → | | **0.05** | **0.13** | **2.1** | **1.6** |
| K | 2021 | 0.202 | 6.00 | 70.9 | 116.0 |
| L | 2021.2 | 0.215 | 5.51 | 73.3 | 121.6 |
| M | 2022 | 0.211 | 5.11 | 73.7 | 121.9 |
| Average → | | **0.21** | **5.54** | **72.6** | **119.8** |
| Stdev → | | **0.01** | **0.45** | **1.5** | **3.3** |

Table 3
Static Elastic Properties of Weir Sandstone

| Sample | Depth (ft) | Poisson's Ratio | Young's Modulus ($x10^6$ psi) |
|---|---|---|---|
| A | 1966 | 0.095 | 2.42 |
| B | 1966.1 | no data | 2.83 |
| C | 1966.2 | 0.107 | 2.88 |
| D | 1966.8 | no data | 2.96 |
| E | 1966.9 | 0.191 | 2.78 |
| F | 1967 | 0.072 | 3.02 |
| G | 1967.1 | 0.130 | 2.79 |
| H | 1967.3 | 0.137 | 3.15 |
| Average → | | **0.12** | **2.85** |
| Stdev → | | **0.04** | **0.22** |
| I | 1967.4 | no data | 3.83 |
| J | 1967.5 | 0.141 | 4.11 |
| Average → | | **0.14** | **3.97** |
| Stdev → | | | **0.20** |
| K | 2021 | 0.081 | 2.65 |
| L | 2021.2 | 0.067 | 2.75 |
| M | 2022 | 0.023 | 2.60 |
| Average → | | **0.06** | **2.67** |
| Stdev → | | **0.03** | **0.08** |

Figure 1
Static Young's Modulus vs Bulk Density

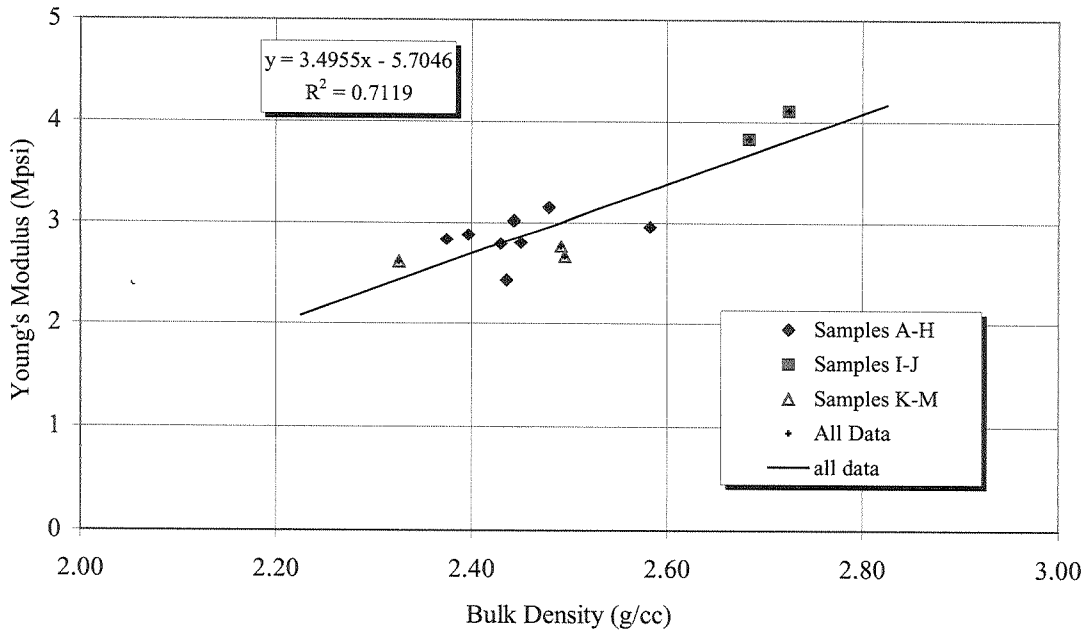


Figure 2
Static Young's Modulus vs P-wave Transit Time

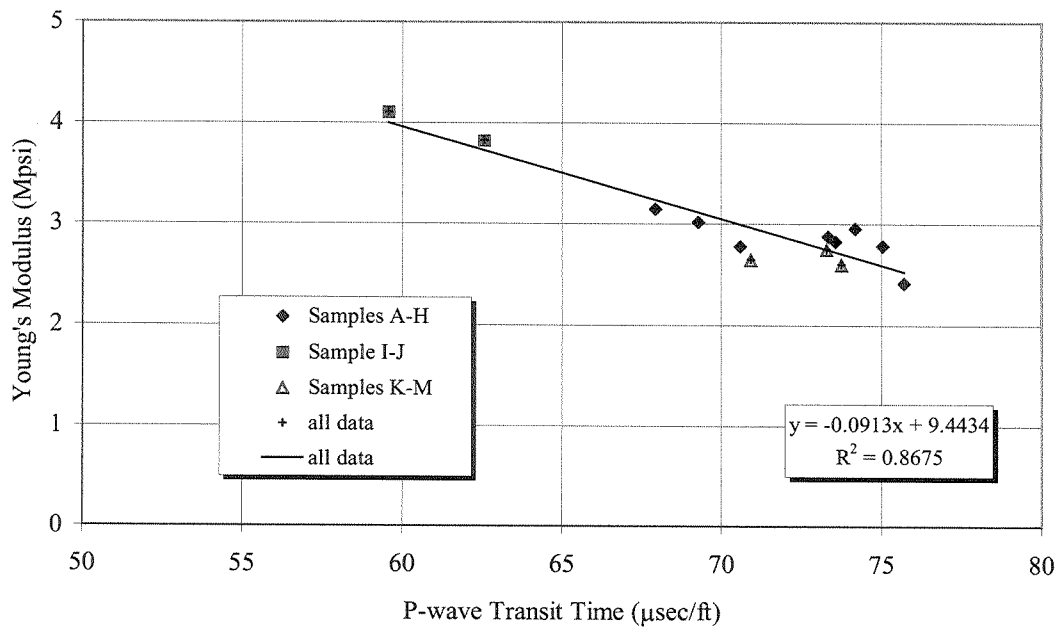

Figure 3
Static vs Dynamic Young's Modulus

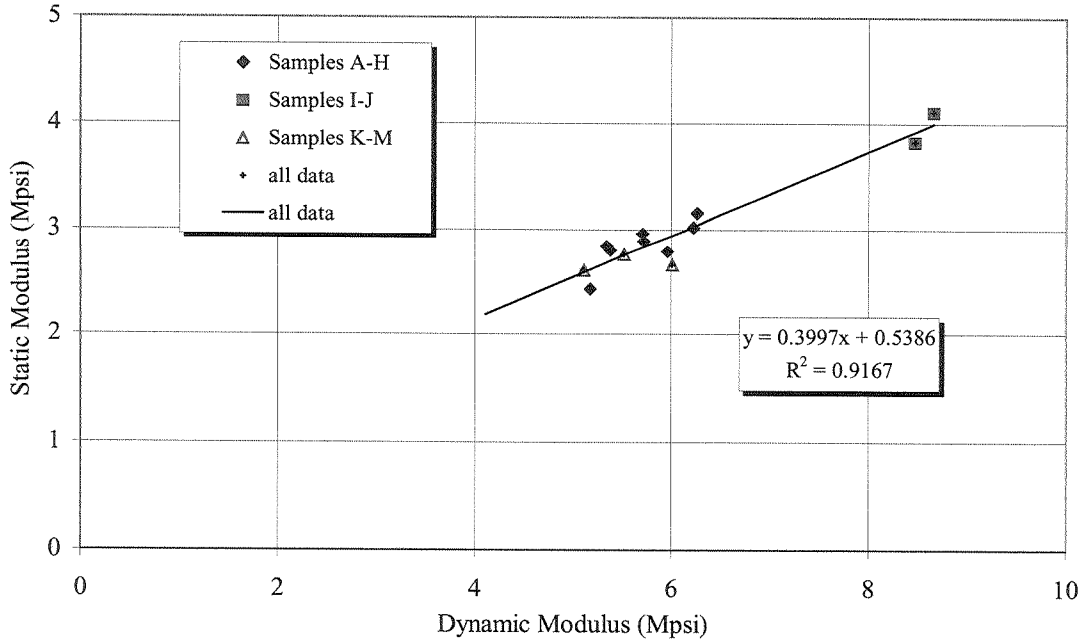


Figure 4
Static vs Dynamic Poisson's Ratio

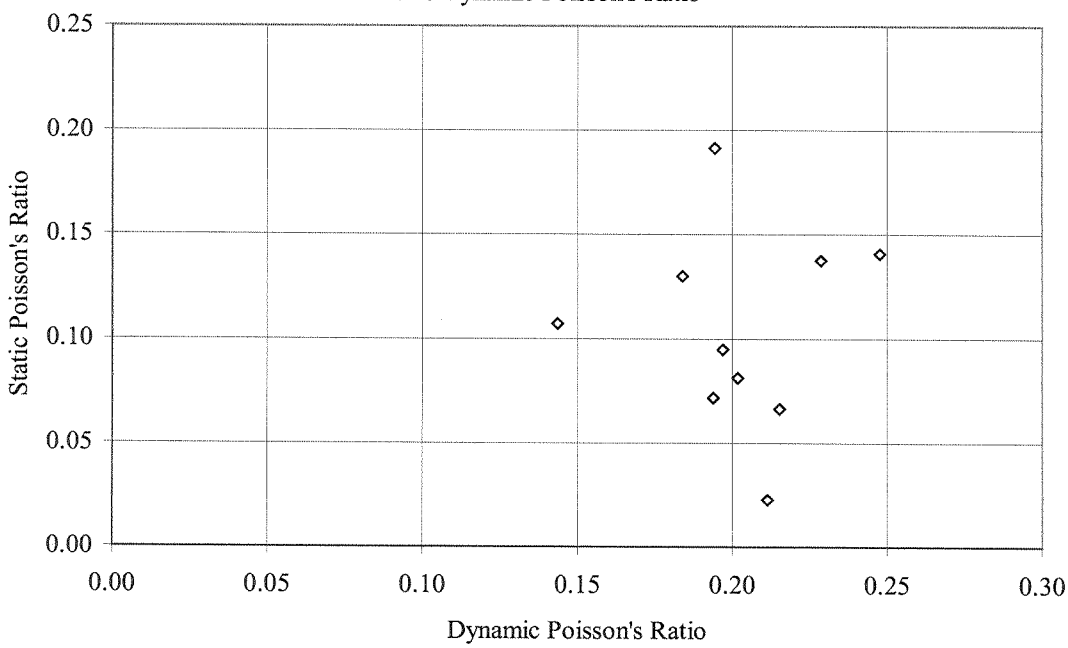

Figure 5
Shear vs Compressional Transit Times

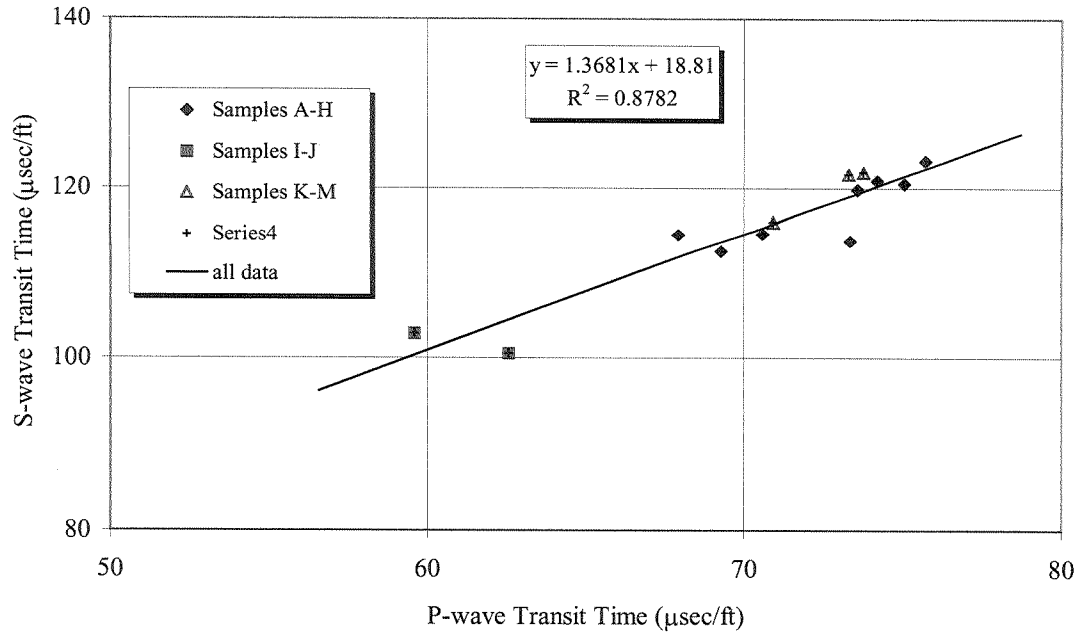

## TEST PROCEDURES

Dynamic Elastic Properties

One-inch diameter cylindrical cores were prepared by grinding the surfaces parallel and smooth to within a tolerance of 0.001 inch. No attempt was made to clean or saturate the core plugs prior to testing.

A non-destructive method of measuring the dynamic elastic properties as a function of axial stress was employed. This was accomplished by measuring the ultrasonic compressional and shear wave velocities using a standard pulsed through-transmission method. Each sample was placed inside a Viton rubber sleeve, and placed between steel platens that housed a pair of polarized s-wave transducers. The rubber sleeve protected the core from the hydraulic oil used to apply the confining pressure. The pressure vessel was mounted in the mechanical press that applied the axial load to the core. The core was initially hydrostatically ramped to 900 psi. The ultrasonic signal was then recorded. The axial load was then increased to 5540 psi and then unloaded back to 900 psi, while maintaining a constant confining stress of 900 psi. The cycle was repeated as second time. The ultrasonic signals were recorded at the 900 psi and 5540 psi axial loads of each cycle. The p-wave transit time was obtained from the mode-converted s-wave signal. The system delay times for the s-wave and p-wave signals were determined from the transit times of their respective propagation modes through an aluminum standard. Knowing the wave velocities of the p-wave and s-wave signals for aluminum, the inherent delay times of each mode were then calculated.

Both the shear wave and compressional wave signals were amplified, band-pass filtered, and displayed on an oscilloscope where the signals' first peak arrival times were measured. The signal peak frequency was 1 MHz. The wave speeds of the compressional and shear modes were calculated by dividing the time of arrival of a particular propagation mode into the length of the sample. Corrections, due to small inherent signal delay times, were applied to the signal arrival times prior to the velocity calculations. The density of each sample was calculated from the ratio of weight to volume, where the bulk volume was calculated from independent caliper measurements of sample length and diameter.

The dynamic Poisson's Ratio and Young's Modulus were calculated from the ultrasonic wave velocities (both p-wave and s-wave) and bulk density using Equations (9) and (10). These relations, although exact only for core materials that possess linear elastic, homogeneous, and isotropic behavior, are employed universally throughout the industry, and usually provide reasonable estimates of the dynamic elastic moduli. The dynamic Poisson's Ratio ($\nu$) was calculated from the expression:

$$\nu = (0.5(V_p/V_s)^2 - 1)/((V_p/V_s)^2 - 1) \qquad (9)$$

$V_p$ and $V_s$ are the compressional and shear wave velocities, respectively. The dynamic Young's Modulus (E) was calculated from the expression:

$$E = 2\rho_b(V_s)^2(1 + \nu) \quad (10)$$

$\rho_b$ is the bulk density of the sample. The results of the stress dependent ultrasonic wave velocities are located in Appendix I.

Static Elastic Moduli

Triaxial or confined tests were performed using a pressure vessel that had a lower one-inch diameter interior steel housing for mounting a sleeved core sample. An upper steel movable piston was inserted into the top portion of the rubber sleeve. The piston contacted the core and extended out the top of the vessel. The pressure vessel was placed on a pedestal in the mechanical press, where the axial load to the core was applied to the movable piston. A circumferential displacement gauge was wrapped around the rubber sleeve and used to measure the change in circumference of the core. Confining stress was supplied by hydraulic oil that fills the vessel and pressurized using a programmable pump. Two LVDT's mounted external to the pressure vessel were used to measure the change in length of the core via displacement of the movable piston.

The stress path followed was identical to that used in measuring the dynamic elastic moduli. In fact, the two measurements were made concurrent to each other. The hydrostatic stress was ramped at a rate of about 175 psi/minute. The axial deviatoric stress was ramped at a rate of 550 psi/minute.

The axial stress was calculated from the ratio of axial force to sample cross-sectional area. The uncorrected axial strain was calculated from the ratio of the average displacements of the two axial LVDT's to the initial sample length. Since the two LVDT's were mounted external to the pressure vessel, the total axial deformation included some deformation from the steel platens and spherical seat of the test frame. The axial strain was corrected by subtracting out the effect of the platens using the relation:

$$\varepsilon_c = \varepsilon_m - \Delta\sigma\, A/(Lb) \quad (11)$$

$\varepsilon_m$ is measured strain, $\Delta\sigma$ is the change in axial stress, A is the sample cross-sectional area, L is the initial sample length, and "b" is the compliance of the platens and test frame, defined as $\Delta F/\Delta x$, where $\Delta F$ is the force required to cause a displacement, $\Delta x$, in the platens and test frame. The "b" compliance factor was actually determined by measuring the Young's modulus of an aluminum standard whose elastic properties are known. "b" was then inferred from the expression:

$$1/E_{al} = 1/E_{al}' - A_{al}/(L_{al}b) \quad (12)$$

The "b" compliance factor was determined over the stress interval at which the Young's modulus was calculated.

Young's modulus (E) was calculated from the slope of the axial stress versus axial strain curve (2nd cycle) between axial stresses of 900 psi and 5500 psi. The stress-strain curves for all samples are displayed in Appendix II.

$$E = \Delta\sigma/\Delta\varepsilon_c \tag{13}$$

The radial strain is expressed as:

$$\varepsilon_r = -\gamma\Delta C/(\pi D) \tag{14}$$

$\Delta C$ is the change in circumference of the sample, which is directly measured by the circumferential LVDT. Note that an increase in circumference (i.e. positive $\Delta C$) produces a negative radial strain. D is the sample's initial diameter. The factor, $\gamma$, is used to compensate for a systematic error (geometric) introduced by the circumferential LVDT. The Poisson's Ratio was calculated from the secant slope of the radial versus axial strain curve between the axial stresses of 900 psi and 5500 psi (2nd cycle).

$$\nu = -\Delta\varepsilon_r/\Delta\varepsilon_c \tag{15}$$

The volumetric strain ($\varepsilon_c + 2\varepsilon_r$) was monitored during the tests. The cores initially go through a compaction phase where the volume of the sample decreases with increasing axial load. As the axial load continues to increase, a point is usually reached where the volume strain begins to increase with additional loading. This turning point in the volume versus axial strain curve represents the start of dilation and the beginning of non-elastic behavior (and sometimes sample failure). This turning point was also used to define the portion of the curve used to calculate the Poisson's Ratio. All calculations of Poisson's Ratio were determined along the compaction portion of the radial versus axial strain curve. The stress-curves of each sample are located in Appendix II.

## REFERENCES

[1] TTC Report No. 04-02-104, "Petrologic Analysis of Wholecore Segments", BJ Davis, S. Heard, June 22, 2004.

| | | |
|---|---|---|
| Technology Center Report No. | **04-02-0104** | Reported by: R.L. Maharidge |
| Requested by: | Roger Myers | |
| Location: | Pittsburgh, PA | |
| Participants: | Nathan Knudson – Sample Prep and Rock Mechanics Tests<br>Russ Maharidge – Data Reduction and Reporting | |
| Distribution: | Roger Myers, Dan Kendrick, Marc Scholl, Bill Wood, Randy LaFollette, TTC file | |

# APPENDIX I

## STRESS DEPENDENT ULTRASONIC WAVE VELOCITY DATA

Table I-A displays the stress dependent inverse compressional and shear wave velocity data for each of the samples. The dynamic Young's Modulus and Poisson's Ratio are also displayed. The values of the transit time and elastic constants reported in Table 2 are the average values of each quantity measured at the reservoir net mean stress shown in bold type in the table below.

Table I-A
Dynamic Elastic Properties of Weir Sandstone Core

| Sample | Net Mean Stress (psi) | Density g/cc | Poisson's Ratio | Young's Modulus (Mpsi) | Inverse P-wave Velocity μsec/ft | Inverse S-wave Velocity μsec/ft |
|---|---|---|---|---|---|---|
| A | 920 | 2.435 | 0.193 | 4.69 | 79.7 | 129.1 |
| | 2412 | 2.435 | 0.249 | 5.90 | 68.1 | 117.8 |
| | 920 | 2.435 | 0.188 | 5.13 | 76.4 | 123.3 |
| | 2412 | 2.435 | 0.246 | 5.93 | 68.1 | 117.4 |
| | 920 | 2.435 | 0.206 | 5.21 | 75.0 | 123.3 |
| | **865** | | **0.197** | **5.17** | **75.7** | **123.3** |
| | | | | | | |
| B | 920 | 2.374 | 0.180 | 4.88 | 77.7 | 124.4 |
| | 2415 | 2.374 | 0.234 | 6.00 | 67.6 | 114.6 |
| | 920 | 2.374 | 0.197 | 5.32 | 73.7 | 120.0 |
| | 2415 | 2.374 | 0.232 | 6.07 | 67.3 | 114.0 |
| | 920 | 2.374 | 0.198 | 5.35 | 73.4 | 119.7 |
| | **865** | | **0.198** | **5.33** | **73.6** | **119.8** |
| | | | | | | |
| C | 922 | 2.396 | 0.126 | 5.24 | 77.0 | 117.8 |
| | 2427 | 2.396 | 0.213 | 6.40 | 66.8 | 110.7 |
| | 922 | 2.396 | 0.150 | 5.73 | 73.0 | 113.9 |
| | 2427 | 2.396 | 0.207 | 6.45 | 66.8 | 109.9 |
| | 922 | 2.396 | 0.137 | 5.70 | 73.6 | 113.5 |
| | **865** | | **0.144** | **5.71** | **73.3** | **113.7** |
| | | | | | | |
| D | 922 | 2.582 | 0.192 | 5.32 | 77.1 | 124.9 |
| | 2427 | 2.582 | 0.242 | 6.53 | 67.1 | 115.0 |
| | 922 | 2.582 | 0.194 | 5.67 | 74.6 | 121.1 |
| | 2427 | 2.582 | 0.243 | 6.58 | 66.8 | 114.6 |
| | 922 | 2.582 | 0.202 | 5.74 | 73.7 | 120.7 |
| | **865** | | **0.198** | **5.70** | **74.2** | **120.9** |

Table I-A
Dynamic Elastic Properties of Weir Sandstone Core

| Sample | Net Mean Stress (psi) | Density g/cc | Poisson's Ratio | Young's Modulus (Mpsi) | Inverse P-wave Velocity µsec/ft | Inverse S-wave Velocity µsec/ft |
|---|---|---|---|---|---|---|
| E | 923 | 2.429 | 0.182 | 5.55 | 73.6 | 118.0 |
| | 2431 | 2.429 | 0.230 | 6.64 | 65.2 | 110.1 |
| | 923 | 2.429 | 0.194 | 5.93 | 70.7 | 114.7 |
| | 2431 | 2.429 | 0.225 | 6.69 | 65.2 | 109.5 |
| | 923 | 2.429 | 0.195 | 5.97 | 70.4 | 114.4 |
| | **865** | | **0.194** | **5.95** | **70.6** | **114.6** |
| | | | | | | |
| F | 922 | 2.443 | 0.225 | 5.38 | 72.9 | 122.4 |
| | 2423 | 2.443 | 0.221 | 6.78 | 65.2 | 108.9 |
| | 922 | 2.443 | 0.193 | 6.18 | 69.5 | 112.7 |
| | 2423 | 2.443 | 0.219 | 6.85 | 64.9 | 108.2 |
| | 922 | 2.443 | 0.195 | 6.26 | 69.0 | 112.1 |
| | **865** | | **0.194** | **6.22** | **69.3** | **112.4** |
| | | | | | | |
| G | 922 | 2.450 | 0.212 | 5.14 | 75.4 | 124.8 |
| | 2423 | 2.450 | 0.227 | 6.22 | 67.8 | 114.1 |
| | 922 | 2.450 | 0.187 | 5.36 | 75.0 | 120.9 |
| | 2423 | 2.450 | 0.229 | 6.30 | 67.3 | 113.4 |
| | 922 | 2.450 | 0.181 | 5.39 | 75.0 | 120.3 |
| | **866** | | **0.184** | **5.37** | **75.0** | **120.6** |
| | | | | | | |
| H | 921 | 2.478 | 0.227 | 5.90 | 70.1 | 117.9 |
| | 2419 | 2.478 | 0.261 | 6.78 | 63.4 | 111.5 |
| | 921 | 2.478 | 0.231 | 6.23 | 67.9 | 114.8 |
| | 2419 | 2.478 | 0.256 | 6.78 | 63.7 | 111.2 |
| | 921 | 2.478 | 0.226 | 6.28 | 67.9 | 114.2 |
| | **866** | | **0.229** | **6.26** | **67.9** | **114.5** |
| | | | | | | |
| I | 922 | 2.684 | 0.174 | 8.15 | 64.1 | 102.0 |
| | 2423 | 2.684 | 0.232 | 8.63 | 60.0 | 101.6 |
| | 922 | 2.684 | 0.195 | 8.51 | 62.0 | 100.7 |
| | 2423 | 2.684 | 0.231 | 8.70 | 59.8 | 101.2 |
| | 922 | 2.684 | 0.173 | 8.43 | 63.1 | 100.3 |
| | **866** | | **0.184** | **8.47** | **62.6** | **100.5** |

Table I-A
Dynamic Elastic Properties of Weir Sandstone Core

| Sample | Net Mean Stress (psi) | Density g/cc | Poisson's Ratio | Young's Modulus (Mpsi) | Inverse P-wave Velocity μsec/ft | Inverse S-wave Velocity μsec/ft |
|---|---|---|---|---|---|---|
| J | 920 | 2.724 | 0.249 | 8.53 | 59.9 | 103.7 |
| | 2415 | 2.724 | 0.272 | 8.61 | 58.3 | 104.1 |
| | 920 | 2.724 | 0.243 | 8.63 | 59.9 | 102.9 |
| | 2415 | 2.724 | 0.271 | 8.68 | 58.1 | 103.7 |
| | 920 | 2.724 | 0.252 | 8.68 | 59.2 | 102.9 |
| | **866** | | **0.248** | **8.65** | **59.6** | **102.9** |
| | | | | | | |
| K | 922 | 2.495 | 0.204 | 5.64 | 73.0 | 119.8 |
| | 2427 | 2.495 | 0.263 | 6.93 | 62.8 | 110.7 |
| | 922 | 2.495 | 0.202 | 6.00 | 70.9 | 116.0 |
| | 2427 | 2.495 | 0.257 | 6.95 | 63.1 | 110.3 |
| | 922 | 2.495 | 0.202 | 6.00 | 70.9 | 116.0 |
| | **889** | | **0.202** | **6.00** | **70.9** | **116.0** |
| | | | | | | |
| L | 924 | 2.491 | 0.198 | 5.16 | 76.6 | 124.9 |
| | 2438 | 2.491 | 0.257 | 6.51 | 65.1 | 113.8 |
| | 924 | 2.491 | 0.213 | 5.48 | 73.6 | 121.8 |
| | 2438 | 2.491 | 0.255 | 6.55 | 65.1 | 113.4 |
| | 924 | 2.491 | 0.218 | 5.54 | 73.0 | 121.5 |
| | **889** | | **0.215** | **5.51** | **73.3** | **121.6** |
| | | | | | | |
| M | 926 | 2.325 | 0.205 | 4.69 | 77.3 | 126.9 |
| | 2446 | 2.325 | 0.254 | 5.75 | 67.2 | 116.9 |
| | 926 | 2.325 | 0.211 | 5.09 | 73.9 | 122.1 |
| | 2446 | 2.325 | 0.245 | 5.77 | 67.6 | 116.2 |
| | 926 | 2.325 | 0.212 | 5.12 | 73.6 | 121.7 |
| | **890** | | **0.211** | **5.11** | **73.7** | **121.9** |

# APPENDIX II

## STRESS-STRAIN CURVES FROM TRIAXIAL TESTS

The following pages contain the stress-strain curves from which Young's modulus and Poisson's Ratio were calculated. Each page contains two figures for a single core plug: (1) top figure - axial stress versus axial strain that was used to determine Young's modulus; (2) bottom figure - radial strain versus axial strain that was used to determine Poisson's Ratio. The portion of the curve used to determine the modulus is shown in "red". The values of the moduli are also displayed in the figures. Note that the strains were set equal to zero at the start of the 1$^{st}$ axial deviatoric load cycle. All moduli were calculated from the increasing axial load of the 2$^{nd}$ cycle. Confining stress equaled 900 psi.

Figure II-1
Young's Modulus of Sample A

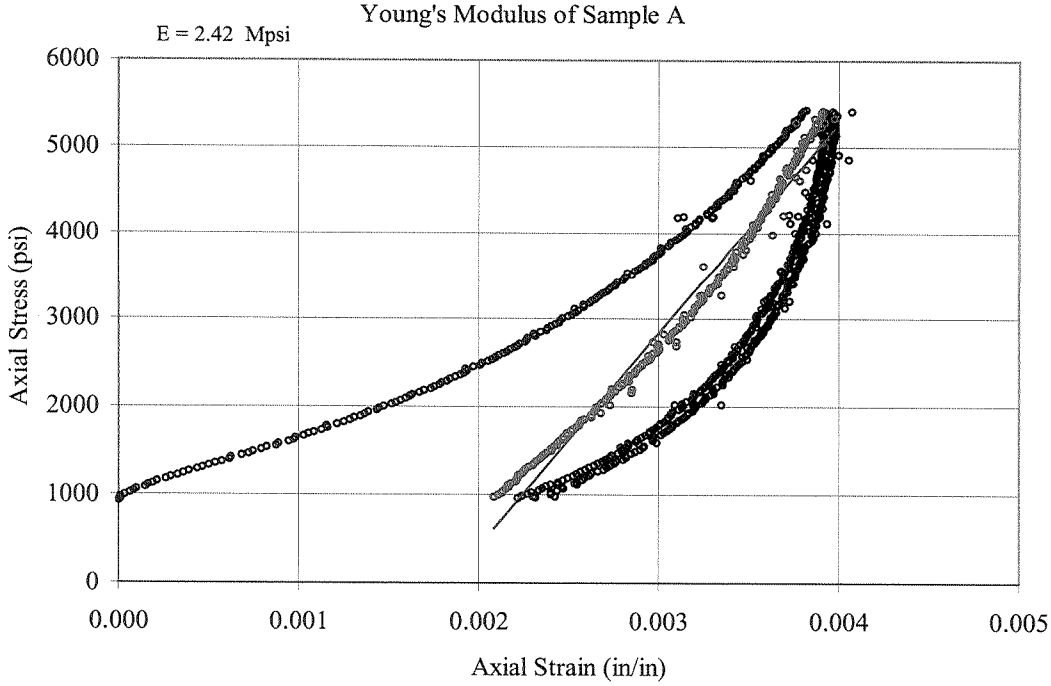


Figure II-2
Poisson's Ratio of Sample A

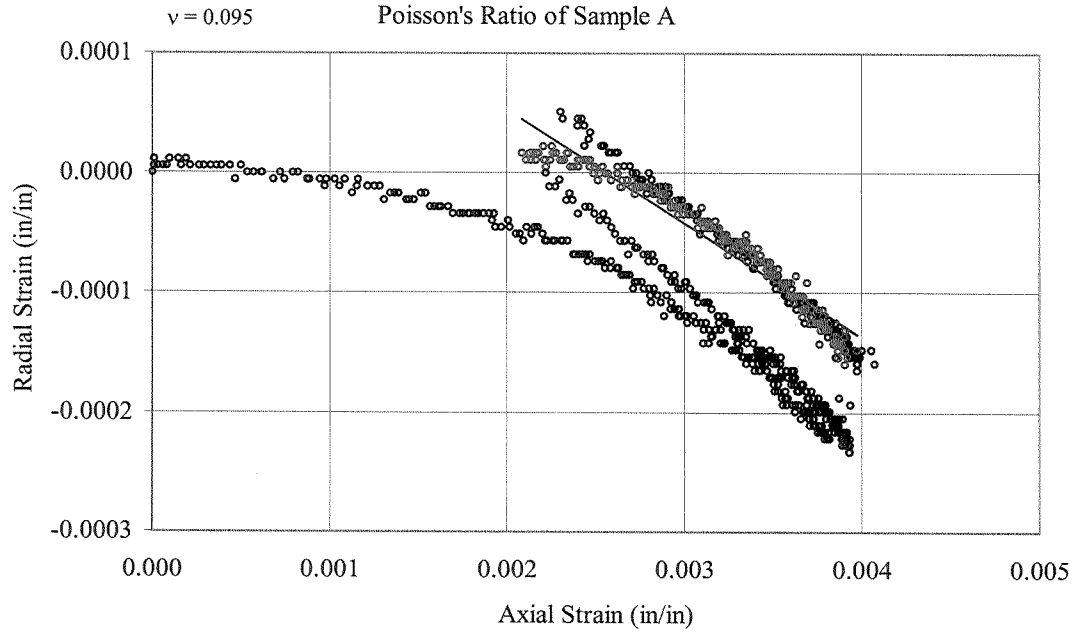

Figure II-3
E = 2.83 Mpsi Young's Modulus of Sample B

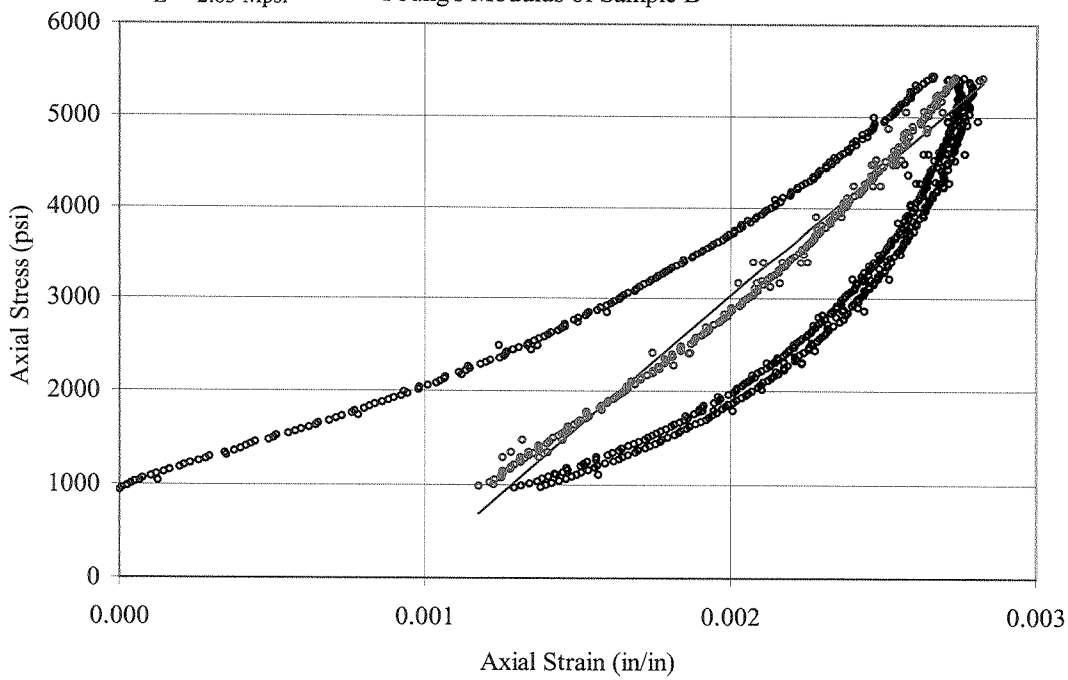

Figure II-4

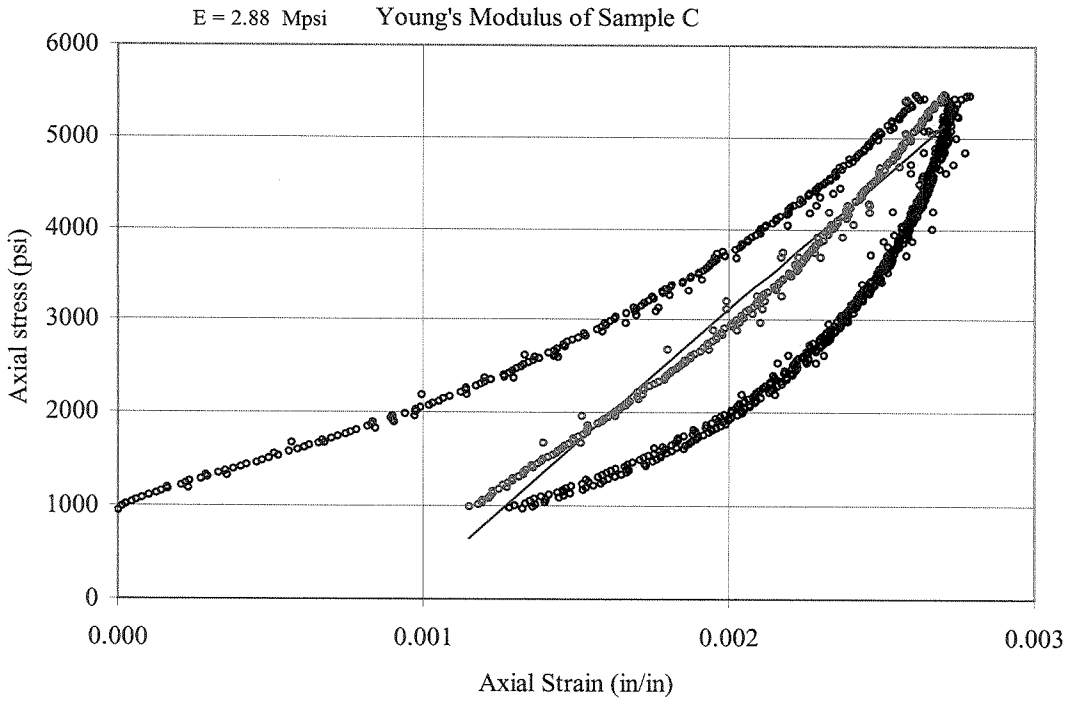


Figure II-5

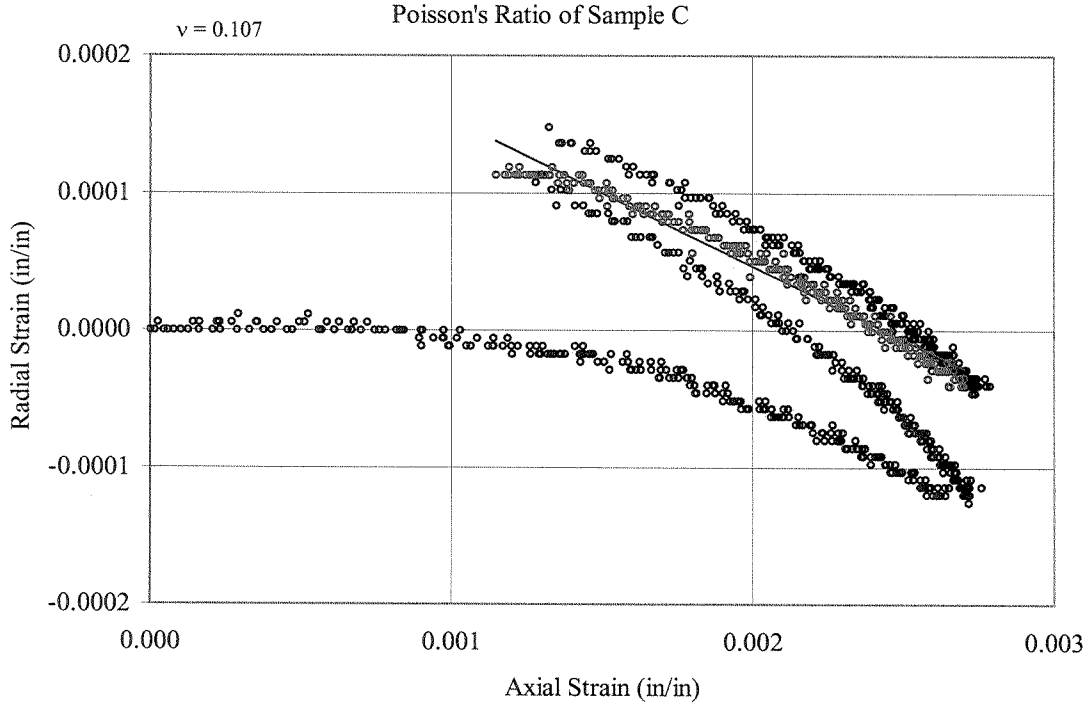

Figure II-6
E = 2.96 Mpsi Young's Modulus of Sample D

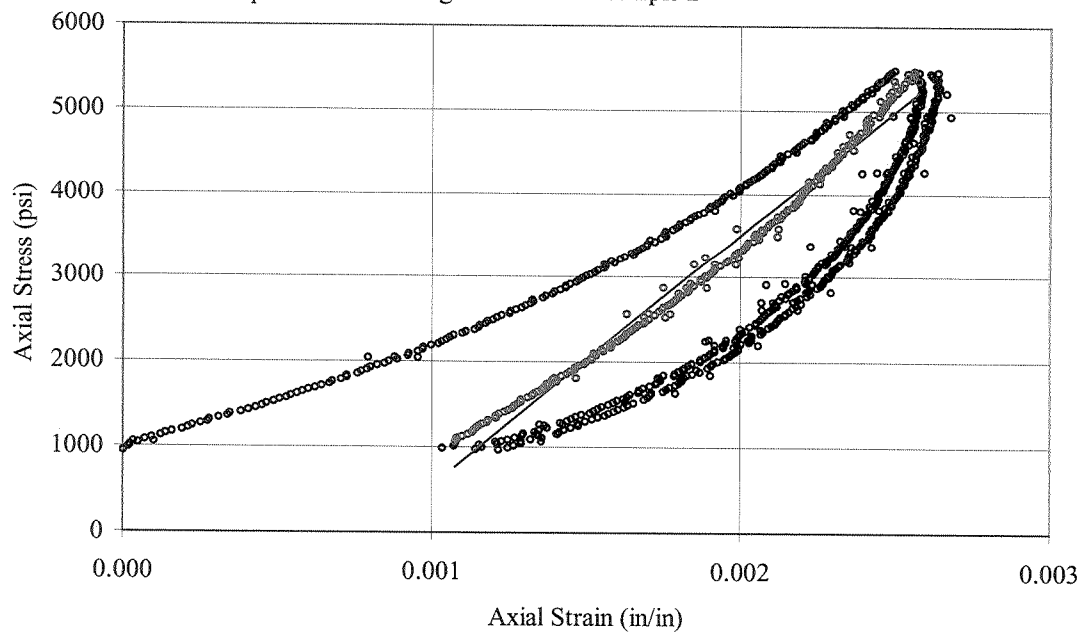

Figure II-7
E = 2.78 Mpsi Young's Modulus of Sample E

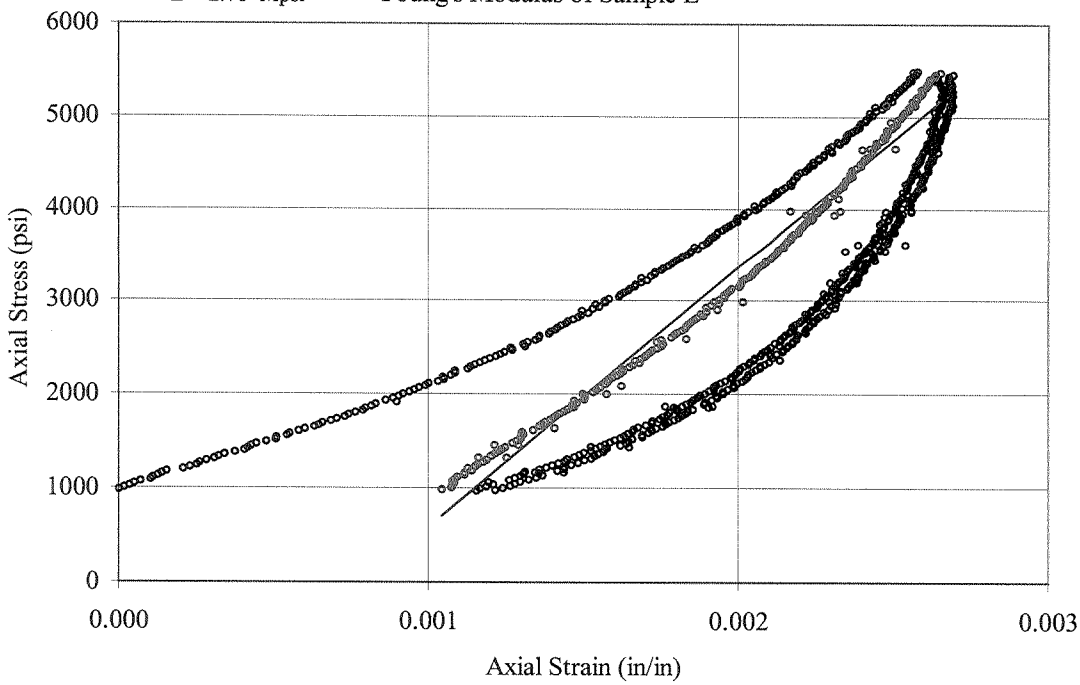


Figure II-8
Poisson's Ratio of Sample E

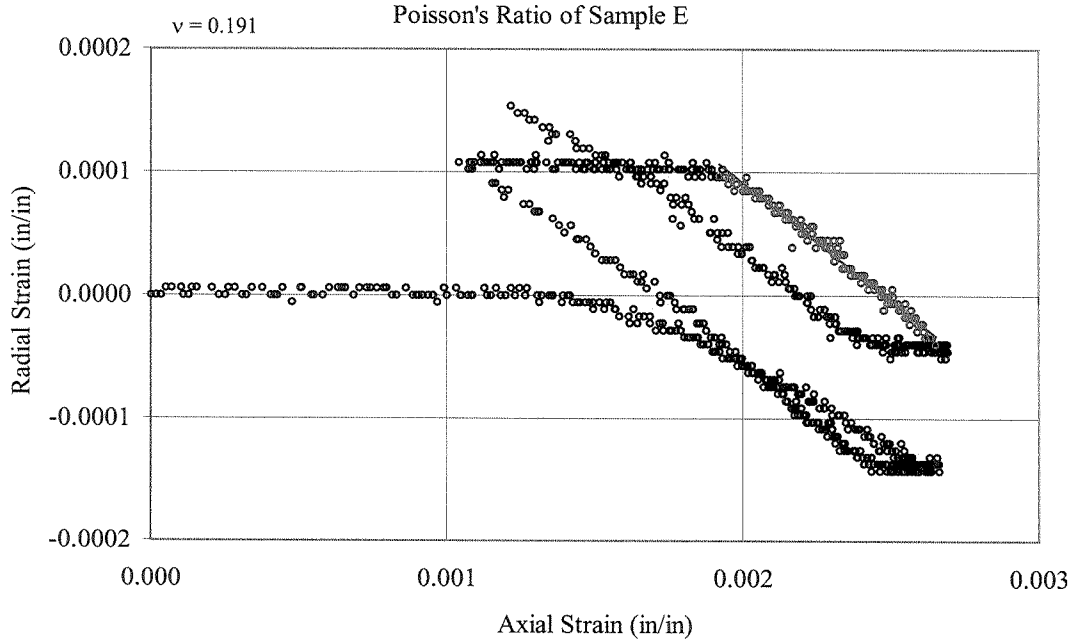

Figure II-9
Young's Modulus of Sample F

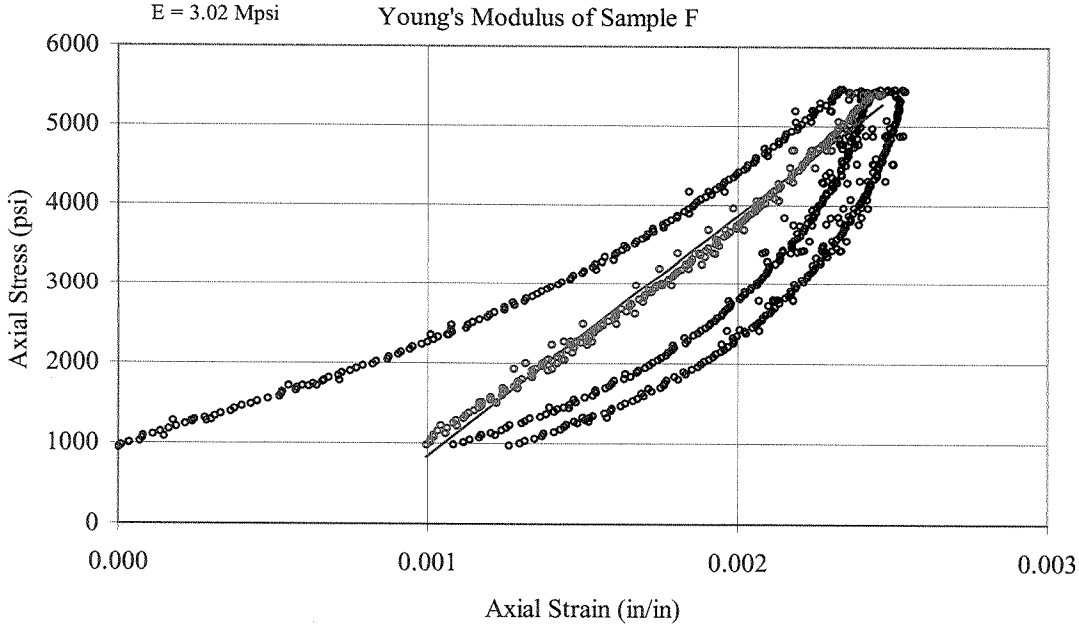


Figure II-10
Poisson's Ratio of Sample F

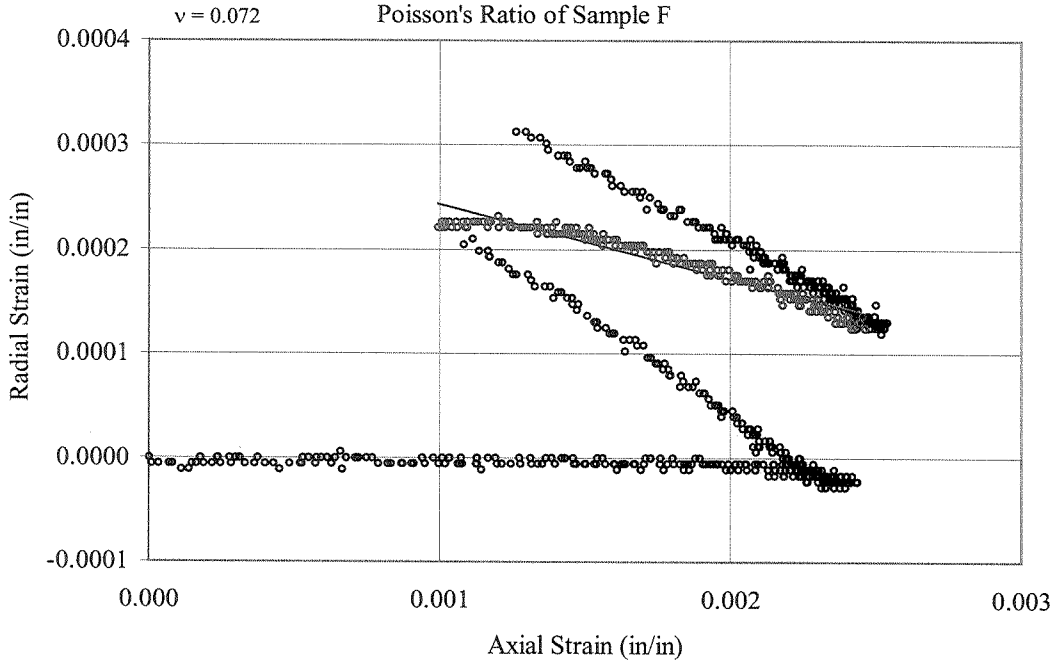

Figure II-11
E = 2.79 Mpsi
Young's Modulus of Sample G

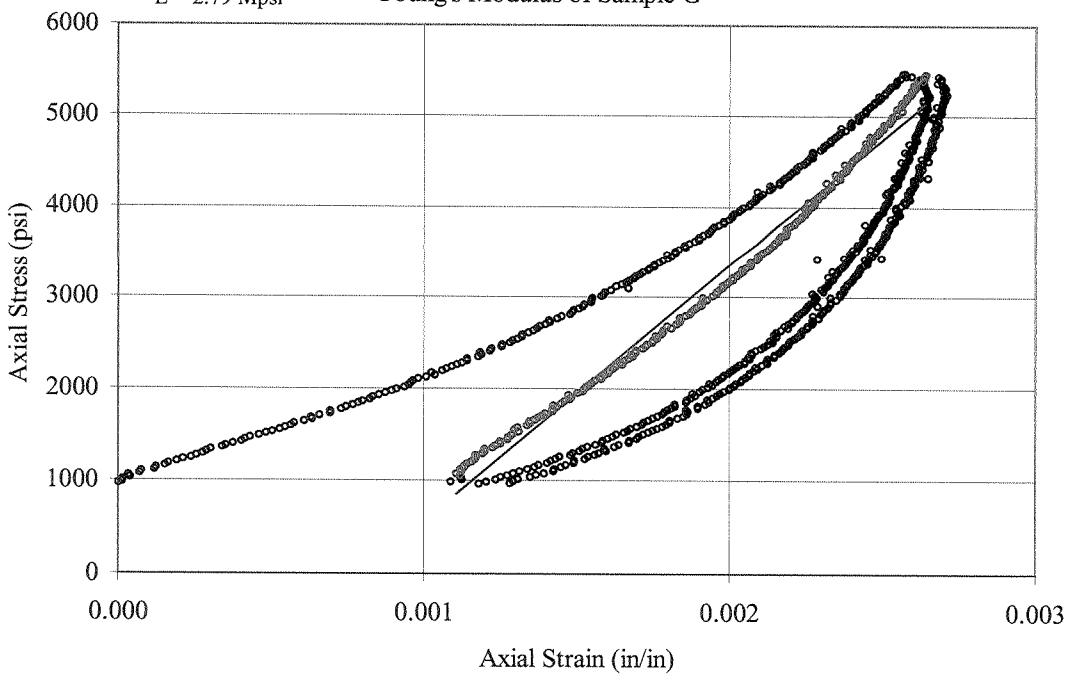


Figure II-12
n = 0.130
Poisson's Ratio of Sample G

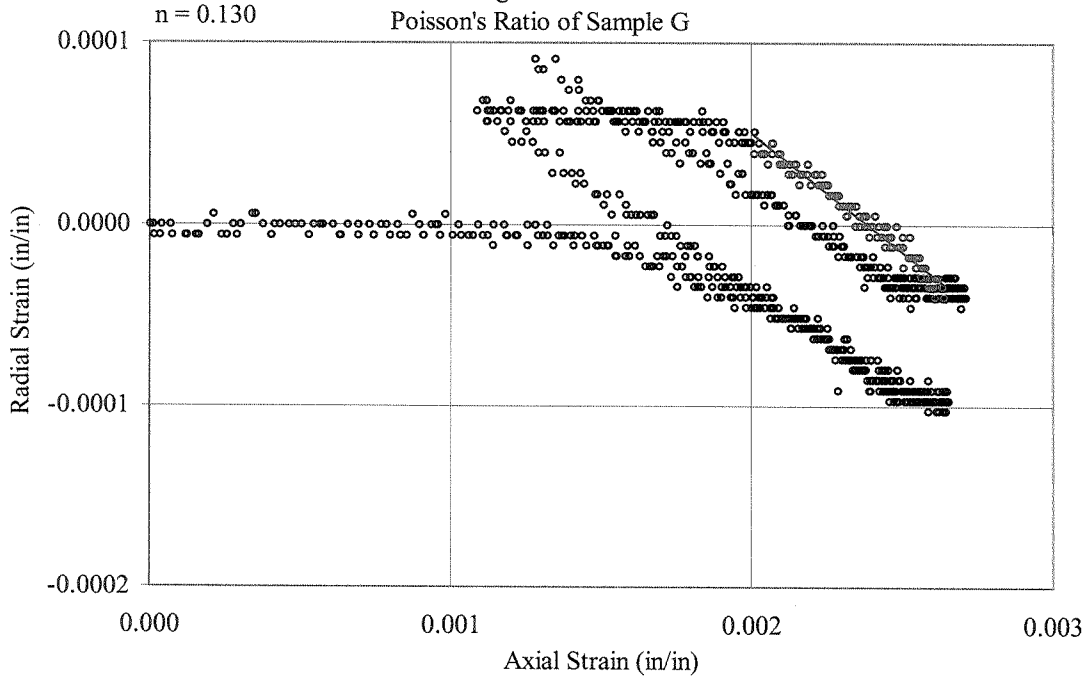

Figure II-13
Young's Modulus of Sample H

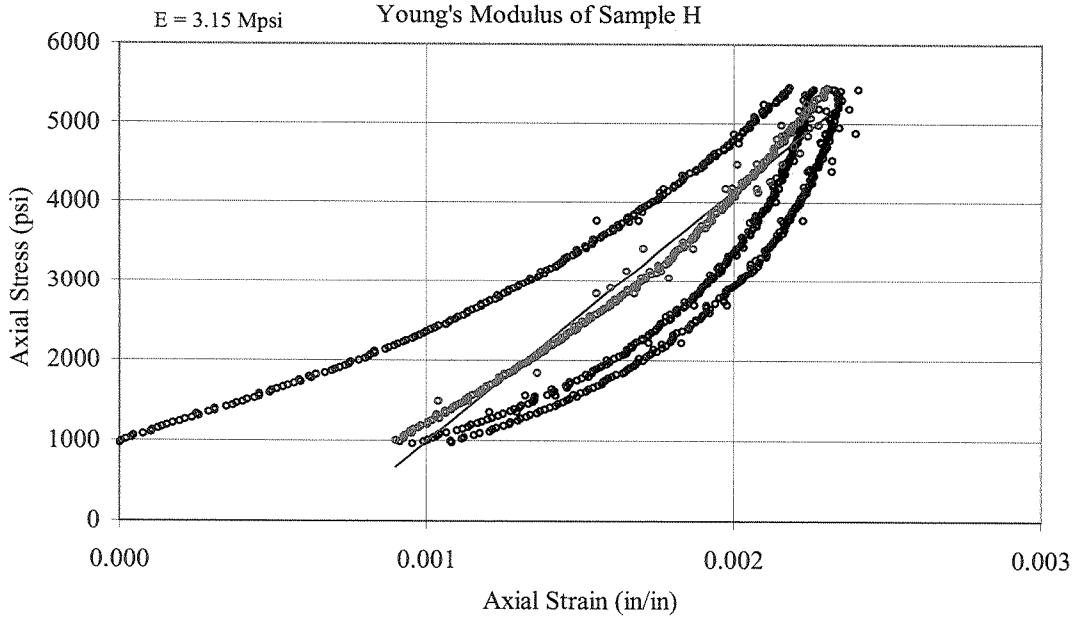


Figure II-14
Poisson's Ratio of Sample H

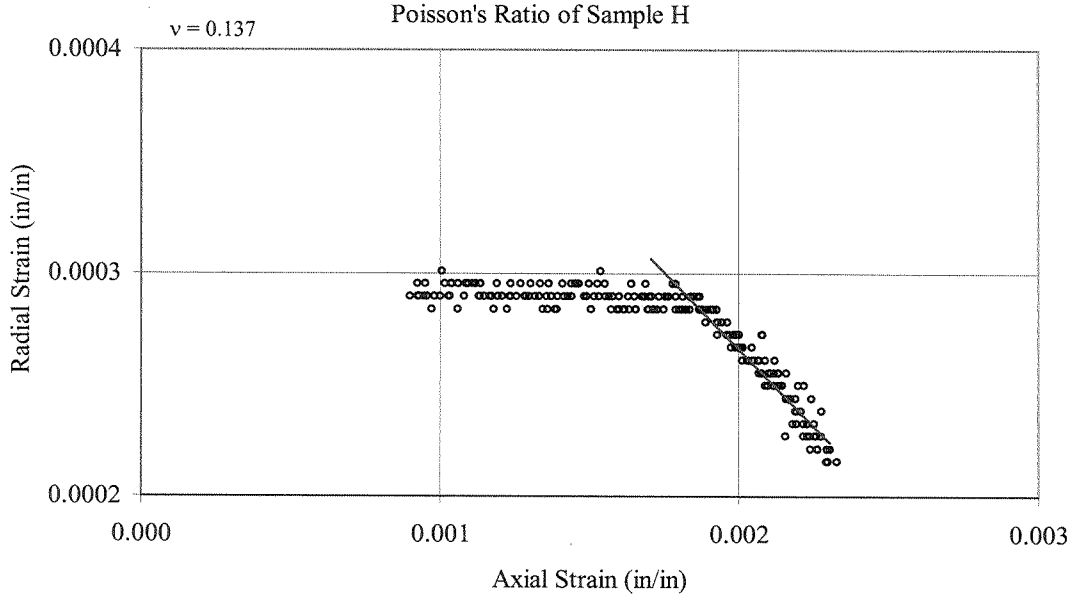

Figure II-15
Young's Modulus of Sample I

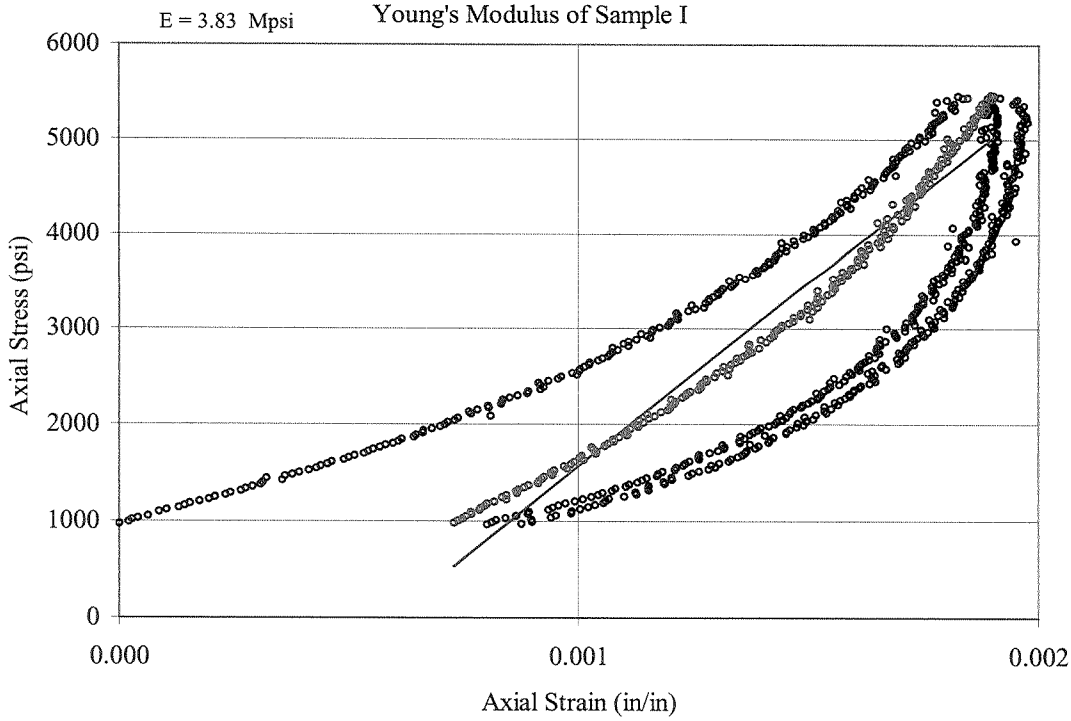

Figure II-16
Young's Modulus of Sample J

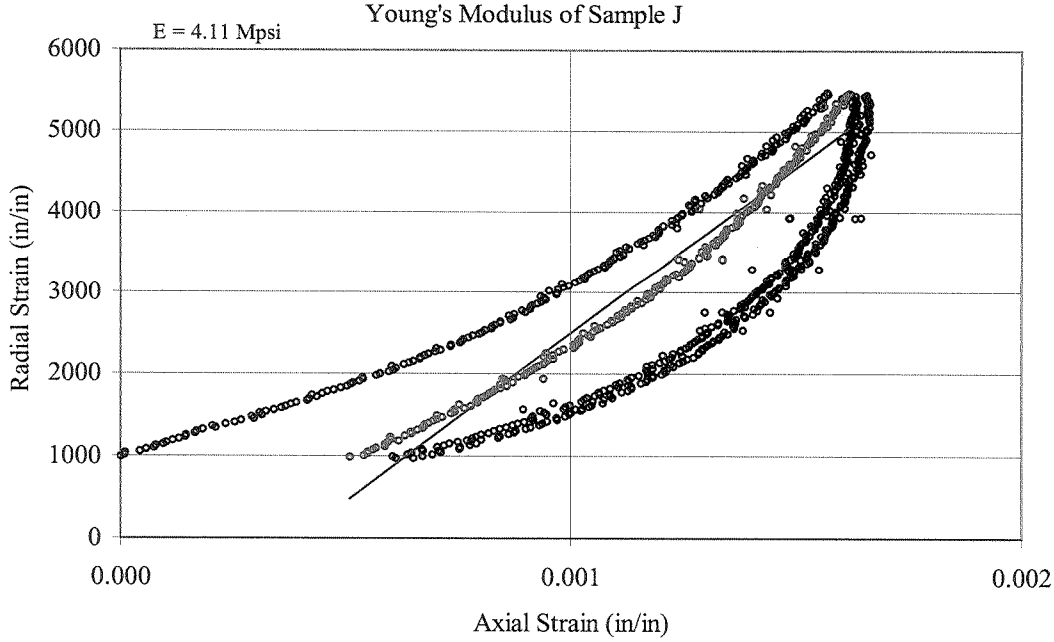


Figure II-17
Poisson's Ratio of Sample J

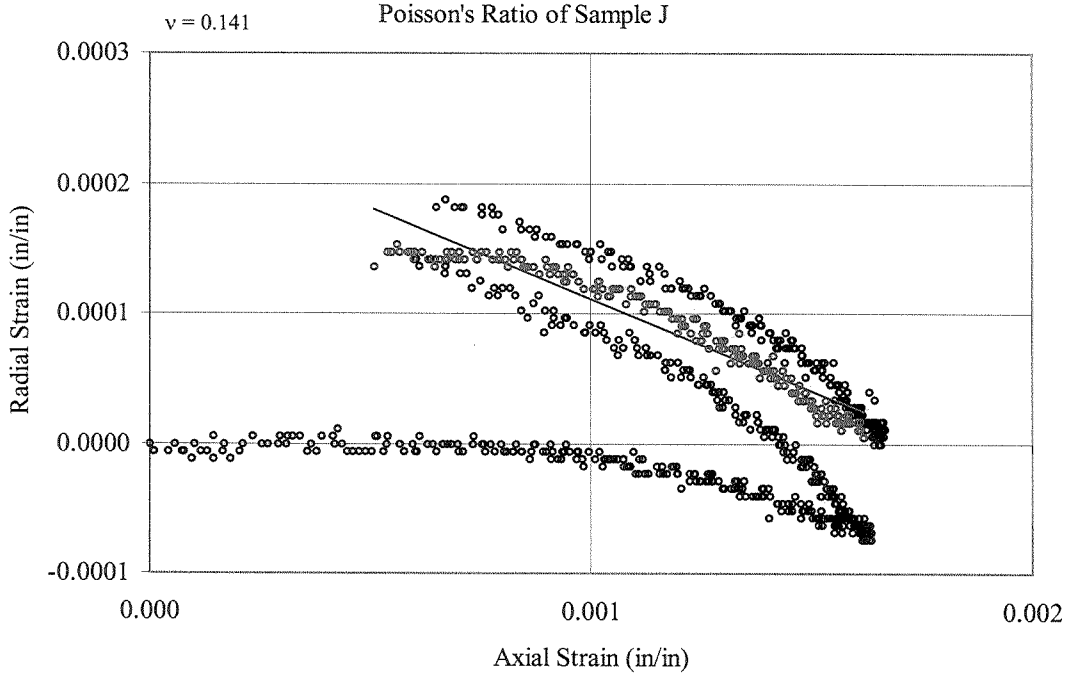

Figure II-18
Young's Modulus of Sample K

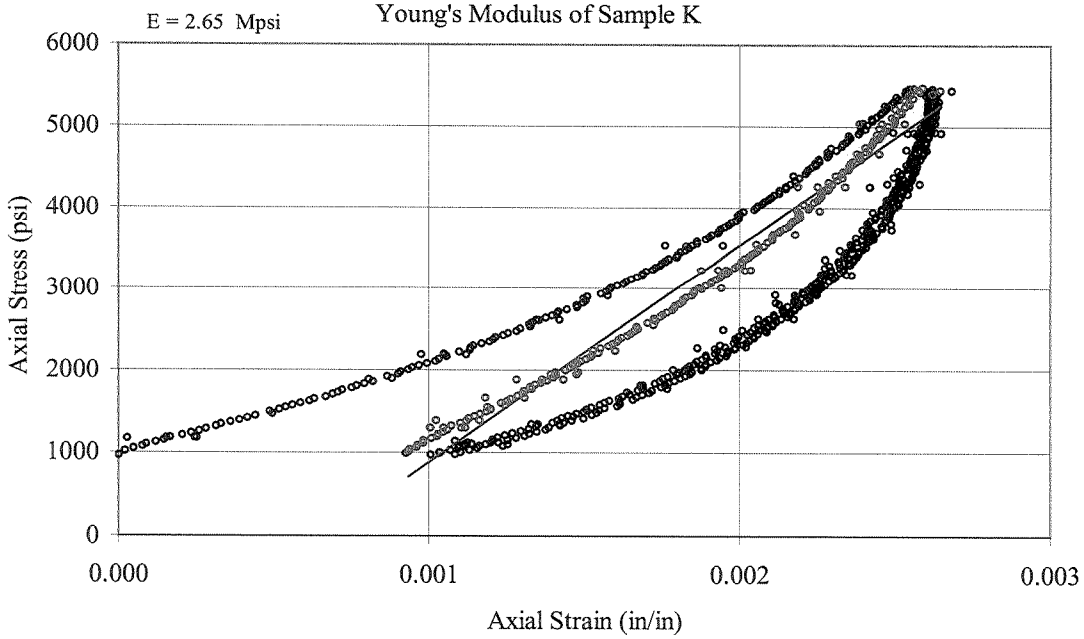


Figure II-19
Poisson's Ratio of Sample K

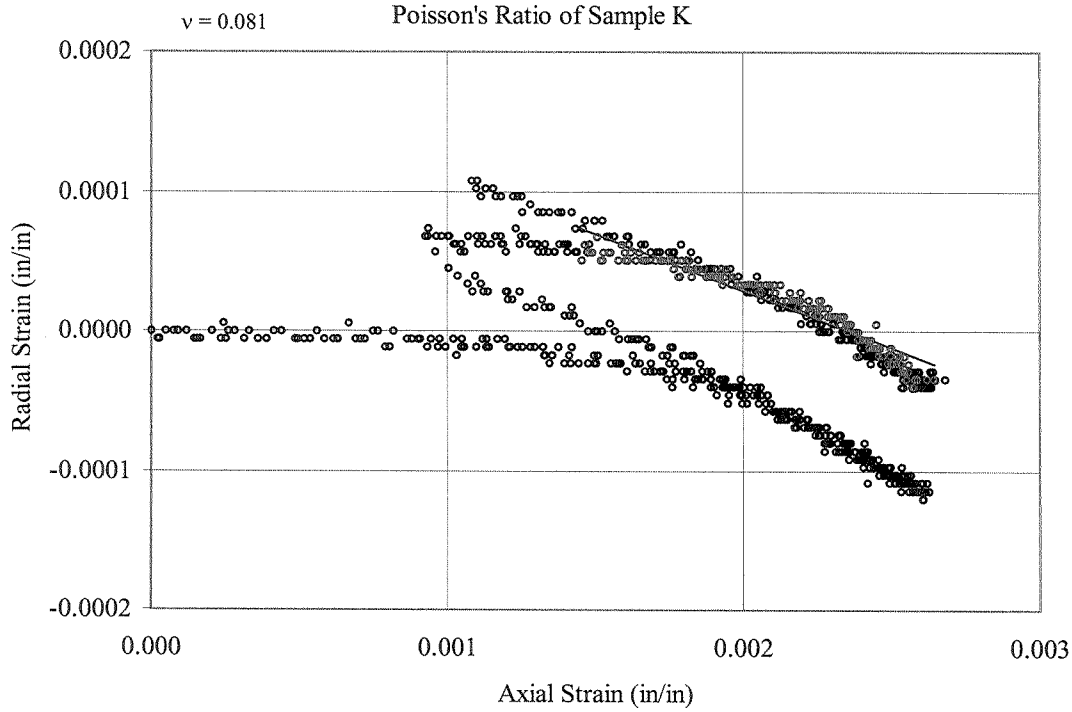

Figure II-20
E = 2.75 Mpsi Young's Modulus of Sample L

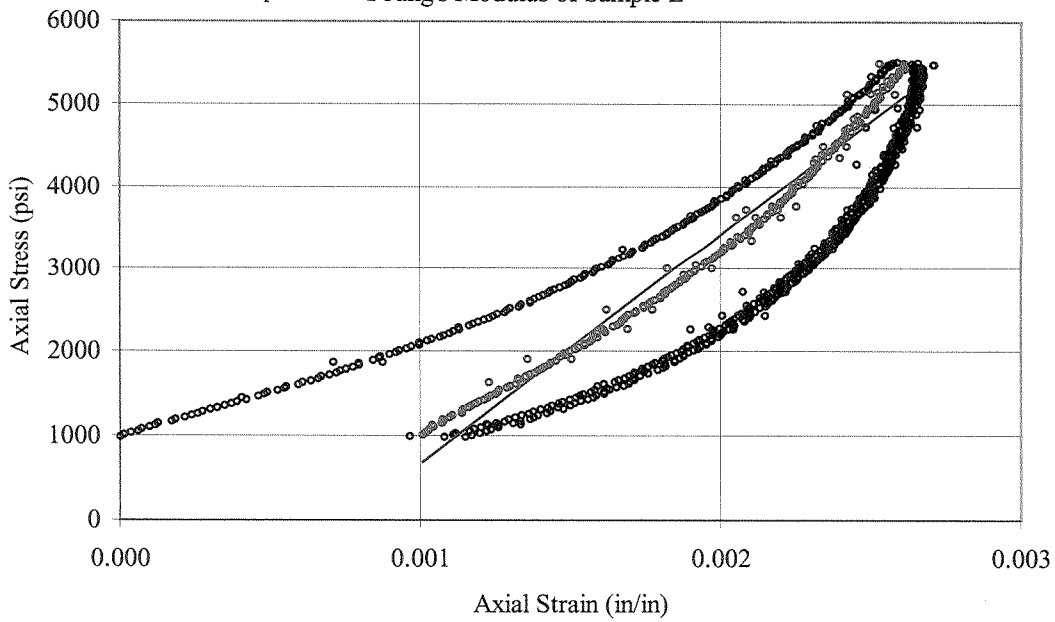


Figure II-21
ν = 0.067 Poisson's Ratio of Sample L

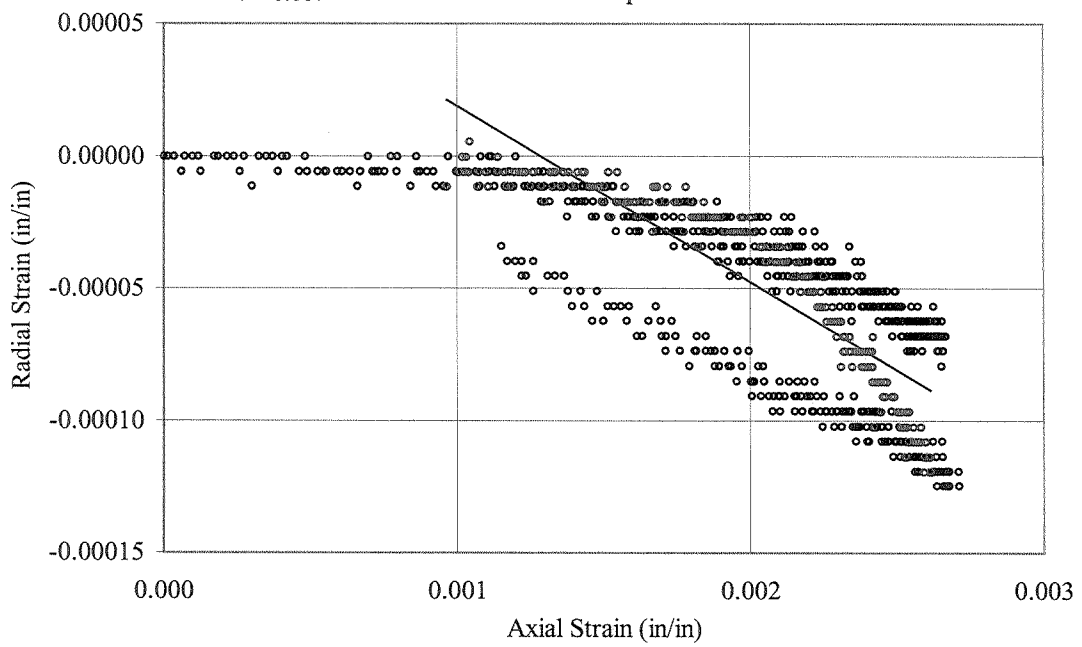

Figure II-22
Young's Modulus of Sample M

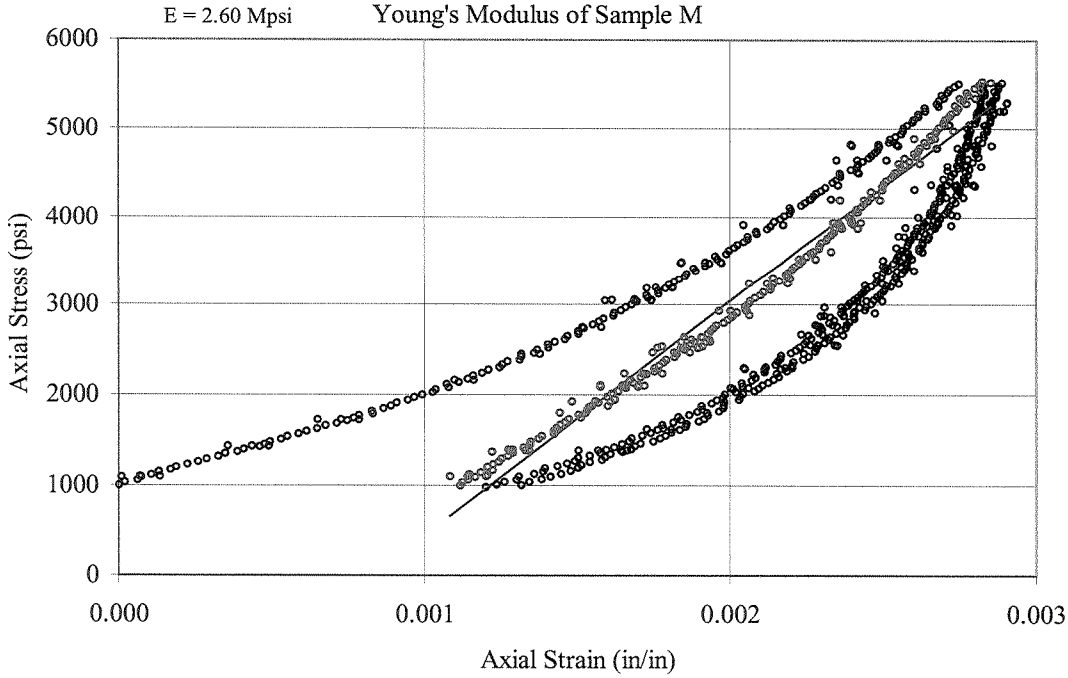


Figure II-23
Poisson's Ratio of Sample M